EUROPEAN ORGANIZATION FOR NUCLEAR RESEARCH
CERN - PS DIVISION

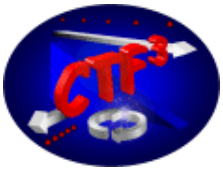

CTF3 Note 040 (MD)
PS/AE Note 2001-020
(Preliminary Phase)

CTF3 Preliminary Phase Commissioning
Report on Third Week, 29 October - 2 November 2001

R. Corsini, B. Dupuy, L. Rinolfi, P. Royer (Ed.), F. Tecker, CERN, Geneva

A. Ferrari, Department of radiation sciences, Uppsala University

M. Belli, C. Milardi, A. Stecchi, INFN - LNF, Frascati

Abstract

In this note, we describe the beam studies done during the third week of commissioning of the Preliminary Phase of CTF3, from October 29^{th} to November 2^{nd} 2001. Detailed optics studies were performed in the linac, with quadrupole scans, trajectory measurements and energy measurements. The beam was then transported in the transfer line for hardware commissioning and some preliminary beam measurements.

Geneva, Switzerland
December 19, 2001

1 Goals

The goal of this week was to study the optics in the linac and to begin the commissioning of the transfer line HIE. We performed optics measurements at various locations in the linac with quadrupole scans and trajectory measurements. We injected the beam in HIE and started preliminary optics studies. The transport in the injection line was done up to the septum magnet HIE.SMH33. Due to hardware failures of the gun, the studies of bunch length using the TCM monitors were postponed.

2 Start-Up

The machine was closed on Monday morning, and hardware tests took place right afterwards. The security chain was checked, with emphasis on the interlock condition on the current of HIE.SMH33. If the current is lower than 1200 A, the beam stopper WL.STP37 shuts down.

On the first day, we checked the polarity of the magnets in the injection line. They all had the right polarity and no modification was mandatory. The MIN/MAX values in the working set were updated for the HIE magnets, according to the equipment limits.

The beam was transported in the transfer line on Monday. However, the diagnostics in the matching section (WL.MSH36 and WL.WBS37), and in the transfer line (HIE.WBS21) were not working properly on this first day, and neither optimisation nor measurement was possible.

During the night from Monday to Tuesday, the modulators were left in pulsing mode at their nominal PFN values, following the specialists' advice. However, MDK27 and MDK31 fell down after a few minutes. The following days, we let them pulsing during the night, but at lower PFN values.

On Tuesday, the first beam was observed in the SEM-grid HIE.MSH23 located in the straight part of the transfer line. Figure 1 shows the first beam profile in HIE.MSH23. The calibration factors used to compute the beam energy and dispersion were not yet implemented in the software.

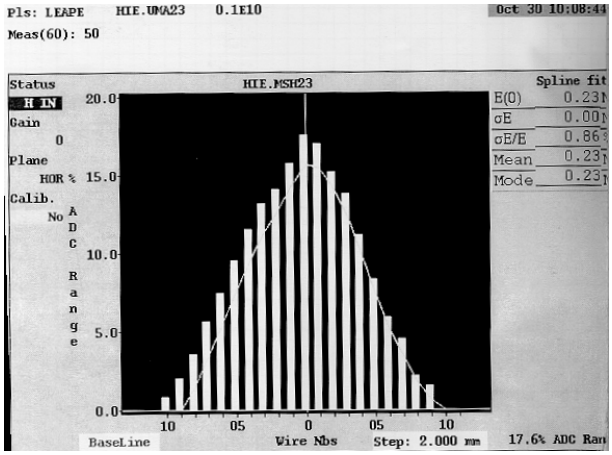

Figure 1: First profile of the beam in the transfer line HIE using the SEM-grid HIE.MSH23.

3 Modulators instability

During the whole week, the modulators MDK27 and MDK31 showed many instabilities, as seen in Figure 2 which shows the history of the output power of MDK27 over a few minutes. Since there is only one acquisition per basic period (1.2 s) on this graph, we had even more trips in the power than recorded on this plot.

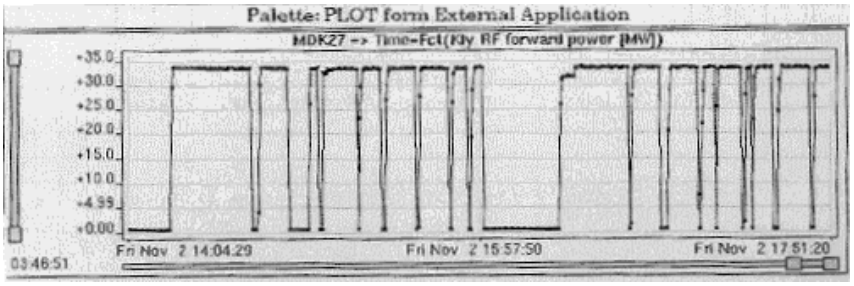

Figure 2: History of the output power of MDK27. Each spike corresponds to a trip.

We recorded the power signals at the output of the klystron-modulators, as shown in Figure 3. We noticed two instabilities. First, we could distinguish two different levels of power on all the three signals. These jumps had periods in the range of a few minutes and were corresponding to random trigger jumps from positive to negative slope at the zero crossing of the 50 Hz signal from the mains. This problem will not occur next year with the new CTF3 timing. Meanwhile, it was solved by modifying the central timing electronics (see details in the following commissioning notes). In addition, we observed that every drop of the MDK27 power was preceded by a sharp increase of the PKI27 signal. An internal protection was making the klystron trip because of some oscillations in the D'Quing system. After changing a thyratron, this problem disappeared.

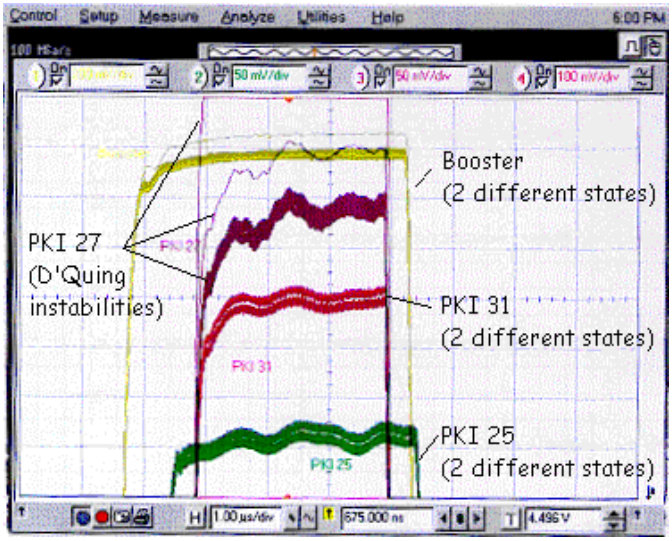

Figure 3: Output power signals of the Booster and the three klystron-modulators. We observed two different states in the power because of the zero crossing jumps, and also the instability on PKI27 due to the D'Quing instability.

While investigating these instabilities, we noticed that the three MDKs were not saturated with the power of 13 kW from the baby klystron. This power was therefore increased to 18 kW. With such a power, MDK27 and MDK31 were saturated and MDK25 (which has a much lower PFN value) was at the limit of saturation. In addition, the baby klystron was changed from Number 1 to Number 2, and the local RF source was replaced by a synthesiser at the frequency $f_0 = 2.99855$ GHz $\pm$ 5 Hz for a power of 15.5 kW (the saturation of the modulators was then verified again).

4 Radiation levels

The background radiation levels were checked by TIS on Monday without beam and with the modulators running at their nominal power, in order to have a reference value for later measurements. On the control room alarm display, all radiation monitors showed levels below 1 μSv/h.

On Tuesday, we made the same recording while sending the beam in the spectrometer line, in the dump line and in the injection line with one pulse, 100×10^8 electrons per pulse at a repetition rate of 50 Hz. As seen in Figure 4, the highest level was reached when sending the beam in the injection line, but was below 5 μSv/h. Later in the week, with different machine settings, a level of 7 μSv/h was reached on the same monitor with the beam in the transfer line.

During an access made on Wednesday, M. Retting from TIS measured 80 μSv/h close to WL.UMA37, and 5 μSv/h close to HIE.MTV23.

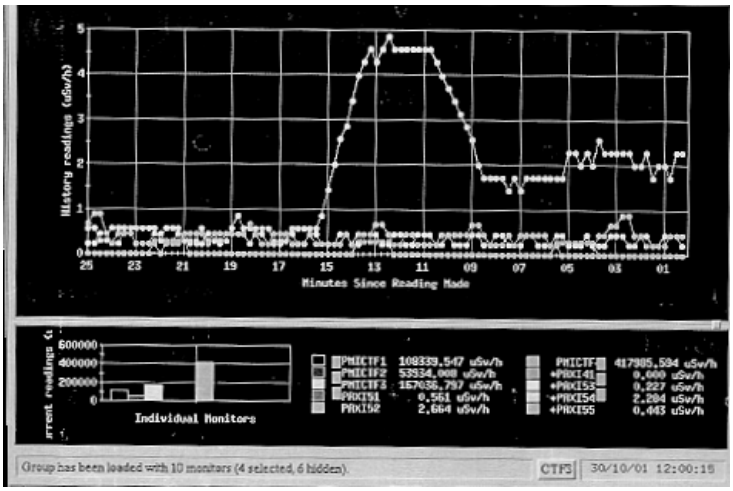

Figure 4: Recording of radiation levels. The first plateau (base line between 15 and 25 minutes on the horizontal axis) corresponds to the beam into the spectrometer line, the second plateau (between 15 and 11 minutes) to the beam into the injection line, and the third plateau (between 9 and 1 minutes) to the beam into the HIP dump line.

5 Beam energy

5.1 Beam energy at the exit of the bunching system

The energy at the buncher output was measured for a klystron power of 4.3 MW, as read by peak power meter. The quadrupoles of the first triplet WL.QSA271, WL.QLA27 and WL.QSA272 were switched off. The current was changed in the steering coils WL.DQSA272H and WL.DQLA27V and the beam position was observed downstream on UMA27. The observed position change is inversely proportional to the beam momentum.

Figure 5 shows that the UMA response is linear in both cases. The position differences due to hysteresis effects were of the same order as the resolution of the UMAs (0.1 mm). With this error, a linear fit resulted in (1.76 ± 0.01) mm/A in the case of WL.DQSA272H and (4.62 ± 0.02) mm/A for WL.DQLA27V. The momentum was calculated using the excitation constants of

$$\frac{\int Bdl}{I} = \begin{cases} 1.14\cdot10^{-4}\ \mathrm{Tm/A} \\ 0.66\cdot10^{-4}\ \mathrm{Tm/A} \end{cases} \text{for} \begin{array}{l} \mathrm{WL.DQLA27V} \\ \mathrm{WL.DQSA272H} \end{array} . \qquad (1)$$

This led to a momentum at the buncher exit of 5.2 and 5.3 MeV/c for the two measurements.

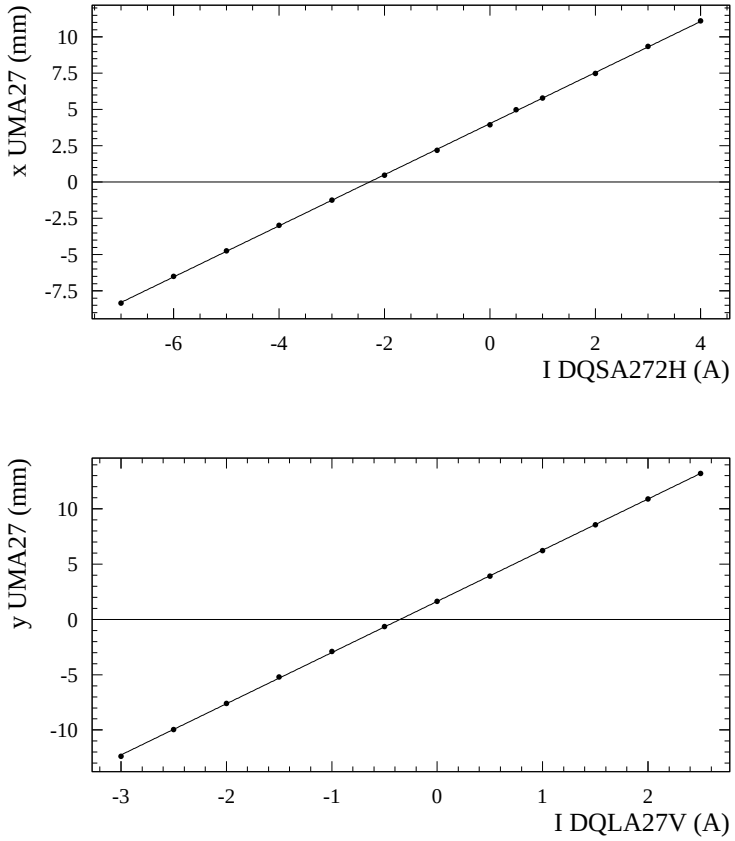

Figure 5: Variation of the beam position on WL.UMA27 as a function of the current in WL.DQSA272H (top) and WL.DQLA27V (bottom).

5.2 Beam energy at the end of the linac

The first measurement of the beam energy after the acceleration sections took place in the spectrometer line, using the spectrometer magnet WL.BHZ36 described in [1]. This method gave an energy of 350 MeV.

Another way to measure the beam energy at the end of the linac is to use the injection line as a spectrometer, using the dipole magnets HI.BSH00 and HIE.BHZ10, which are of the same type. Equation (2) gives the integrated field in HI.BSH00 or HIE.BHZ (in T.m) as a function of the current in the magnet (in A). Figure 6 shows the magnetic measurement points and the calibration curve as a function of the current in HI.BSH00 or HIE.BHZ.

$$\begin{aligned} \int B\mathrm{d}l = \; & + \; 6.402828 \times 10^{-4} \\ & + \; 1.467235 \times 10^{-3} \times I \\ & + \; 3.133053 \times 10^{-7} \times I^2 \\ & - \; 1.626597 \times 10^{-9} \times I^3 \\ & + \; 3.603325 \times 10^{-12} \times I^4 \\ & - \; 3.105279 \times 10^{-15} \times I^5 \end{aligned} \tag{2}$$

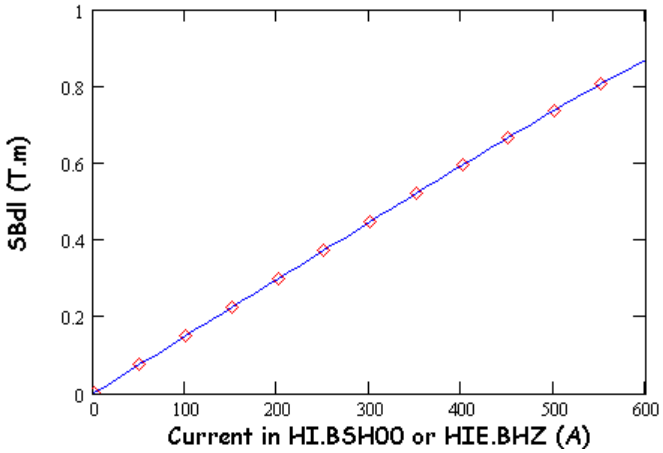

Figure 6: Magnetic measurements and calibration curve for the dipole magnets in the injection line HI.BSH00 and HIE.BHZ.

The principle of the measurement is to rely on the geometrical design of the injection line with a first angle of 9 degrees given by HI.BSH00 and a second angle of 20 degrees given by HIE.BHZ10. First, the steering at the end of the linac was adjusted such that the beam entered the first magnet on the central orbit. Then, by looking at the beam in HIE.MTV01, we adjusted the current in HI.BSH00 to be centred in WL.MTV01. The current was then $I_{BSH} = 115.5$ A, thus corresponding to a beam energy of 332 MeV. We checked that this setting was also valid for the HIP dump line which has the same geometry: we inverted the polarity in HI.BSH00 and observed the beam centred in HIP.MTV01. Since the dipole magnets HI.BSH00 and HIE.BHZ10 are of the same type, the ratio of the currents in the magnets is the ratio of the deflection angles, say $I_{BSH}/I_{BHZ} = 9/20 = 0.45$. We then powered HIE.BHZ10 with the new current value $I_{BHZ} = 115.5/0.45 = 256.7$ A, and observed that the beam was also centred in the following screen HIE.MTV23. All the quadrupoles were on stand-by during these manipulations.

This discrepancy of 5% in the final energy between the spectrometer line and the injection line remains to be clarified.

6 Beam Diagnostics

During the week, a systematic check of the instrumentation took place, and we noticed the following points:

- WL.WBS28 had horizontal and vertical planes inverted.
- WL.WBS31 had horizontal and vertical planes inverted. We observed that the horizontal profile was moving when powering the steerer WL.DQNF301V. This was confirmed by using the magnet WL.DQNF302H in the other plane.
- WL.WBS37 was successfully tested in both planes using the steerers WL.DQNF353V and WL.DQNF352H. However, WL.WBS37 is mounted reversed because of limited space and the horizontal plane is inverted.
- HIE.WBS21 only showed a very small signal in the vertical plane and no signal in the horizontal plane. However, the beam conditions were far from being optimised in the injection line during this test. The wire displacement was only 5 mm instead of 10 mm on the other wire beam scanners.
- WL.MSH36 had the high energies displayed on the left-hand side of the profile.

– HIE.MSH23 worked properly, although the energy reading was not correct because the calibration factors were missing in the software.
– All the MTVs were adjusted to cope with the nominal beam intensity. An access was made in order to reduce some of the diaphragms. The optics on HIE.MTV30 was changed.

All the mandatory modifications on the diagnostic tools were made during the week.

7 Transverse beam dynamics in the linac

7.1 Description of the linac geometry

In the CTF3 preliminary phase, the linac consists of eight accelerating sections, referred to as ACS27 to ACS34. Quadrupoles are installed on and between these accelerating sections in order to focus the beam on its path. At the end of the linac, the electron beam is matched to the conditions required by the HIE line and by the EPA ring [2]. Five independent quadrupoles are used for this purpose. Also, some instrumentation is installed at various locations along the linac in order to measure the Twiss parameters, the position and the energy of the beam. In this section, we shall focus on the measurement of the lattice parameters by performing quadrupole scans and observing the transverse beam size in the wire beam scanners WL.WBS31 (located between ACS30 and ACS31) and WL.WBS37 (located in the matching section).

7.2 Quadrupole scans in the matching section

One of the first purposes of the transverse measurements in the linac is to check the Twiss parameters at the exit of the last acceleration section. One can then calculate the normalised gradients in the quadrupoles of the matching section, in order to have a matched beam at the entrance of the injection line.

As described in Section 5.2, two different methods for the energy measurement resulted in different values (332 MeV and 350 MeV). In the following, the results are presented for both energies.

In order to measure the rms transverse beam size, we fit the beam profile with a function which is either $f_1(d) = cste + G_1(d)$ or $f_2(d) = cste + G_1(d) + G_2(d)$, where G is a Gaussian function and d is the displacement of the wire through the beam. After removing the constant term, one can easily obtain the rms beam size of the profile in a given direction, as a function of the current in a quadrupole Q upstream. A three parameter function is then used to fit this scan in order to derive the Twiss parameters and the emittances at the entrance of Q. Four quadrupole scans were performed in WL.WBS37 after having optimised the acceleration phases for peak power meter readings of 4.2, 34.0 and 34.6 MW on MDK25, MDK27 and MDK31. Table 1 summarises the quadrupole conditions used for the scans in WL.WBS37.

	I_{QNF351} [A]	I_{QNF352} [A]	I_{QNF353} [A]
Horizontal and Vertical Scan using WL.QNF351	15 to 100 (H) -50 to 10 (V)	73.2	54.6
Horizontal Scan using WL.QNF352	35.5	5 to 95	54.6
Vertical Scan using WL.QNF352	-45	10 to 90	54.6

Table 1: Quadrupole currents in the triplet of the matching section during the quadrupole scans in WL.WBS37.

The Twiss parameters and the normalised rms emittances at the entrance of WL.QNF351 that we derived from these measurements are given in Table 2. The function used to fit the transverse beam profiles does not have a significant influence on our results.

Lattice parameters	Fit with one Gaussian	Fit with two Gaussians
Horizontal Scan using WL.QNF351		
β_x (m)	19.8	18.2
α_x	+0.95	+1.15
ϵ_x (mm.mrad)	24	27
Horizontal Scan using WL.QNF352		
β_x (m)	25.0	17.4
α_x	+1.22	+1.11
ϵ_x (mm.mrad)	31	25
Vertical Scan using WL.QNF351		
β_y (m)	16.2	13.5
α_y	-2.06	-1.69
ϵ_y (mm.mrad)	18	25
Vertical Scan using WL.QNF352		
β_y (m)	21.2	17.2
α_y	-2.77	-2.28
ϵ_y (mm.mrad)	18	26

Table 2: Twiss parameters and normalised rms emittances at the entrance of WL.QNF351 derived from quadrupole scans in WL.WBS37. The energy is here 350 MeV.

Quadrupole		Reference 350 MeV	350 MeV	332 MeV
WL.QNF351	β_x [m]	9.0	17.4	16.5
	α_x	+1.7	+1.11	+0.94
	β_y [m]	12.1	21.2	19.7
	α_y	-2.5	-2.77	-2.92
WL.QLB29	β_x [m]	-	37.8	33.2
	α_x	-	-3.28	-4.03
	β_y [m]	-	27.1	17.6
	α_y	-	-2.20	-1.63

Table 3: Twiss parameters at the entrance of WL.QNF351 and WL.QLB29 for two different energies. The reference 350 MeV column gives the nominal values of the theoretical optics. The 350 MeV and 332 MeV columns are the values, which best fit the measurement points.

Table 3 displays the Twiss parameters found at two different locations for two different energies at the end of the linac. In all these cases, the normalised rms emittances are close to 20π mm.mrad in both planes. Figure 7 is an example of the variations of the horizontal and vertical rms beam size measured in WL.WBS37 as a function of the current in the upstream quadrupole WL.QNF352. The solid lines show the result of the fit used to derive the emittance and the Twiss parameters.

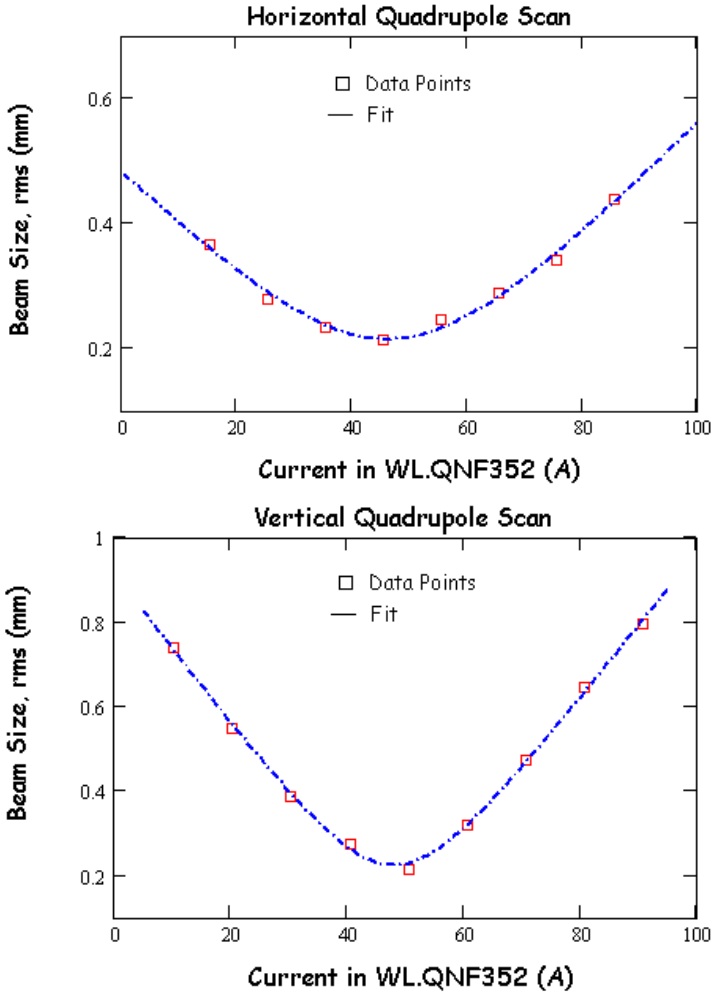

Figure 7: Quadrupole scans in WL.WBS37 using WL.QNF352. The fit is done with an energy of 332 MeV.

7.3 Quadrupole scans with WL.WBS31

Since the lattice parameters at the entrance of WL.QLB29 could be derived from the quadrupole scans in the matching section, a second series of transverse measurements, more upstream in the linac, was performed in order to check the consistency of our results.

- The current in the quadrupoles of the QNFB family was set to 27 A, and we made a horizontal and vertical scan in WL.WBS31 using WL.QLB29.
- The current in the quadrupoles of the QNFB family was set to 20 A, and we made a vertical scan in WL.WBS31 using WL.QLB29.

Figure 8 shows that there is a good agreement between the experimental and simulated quadrupole scans (with both 332 and 350 MeV for the energy in the matching section). We are thus confident that the model used in order to simulate the optics in the linac and to predict the behaviour of the beam in the transverse plane is reliable.

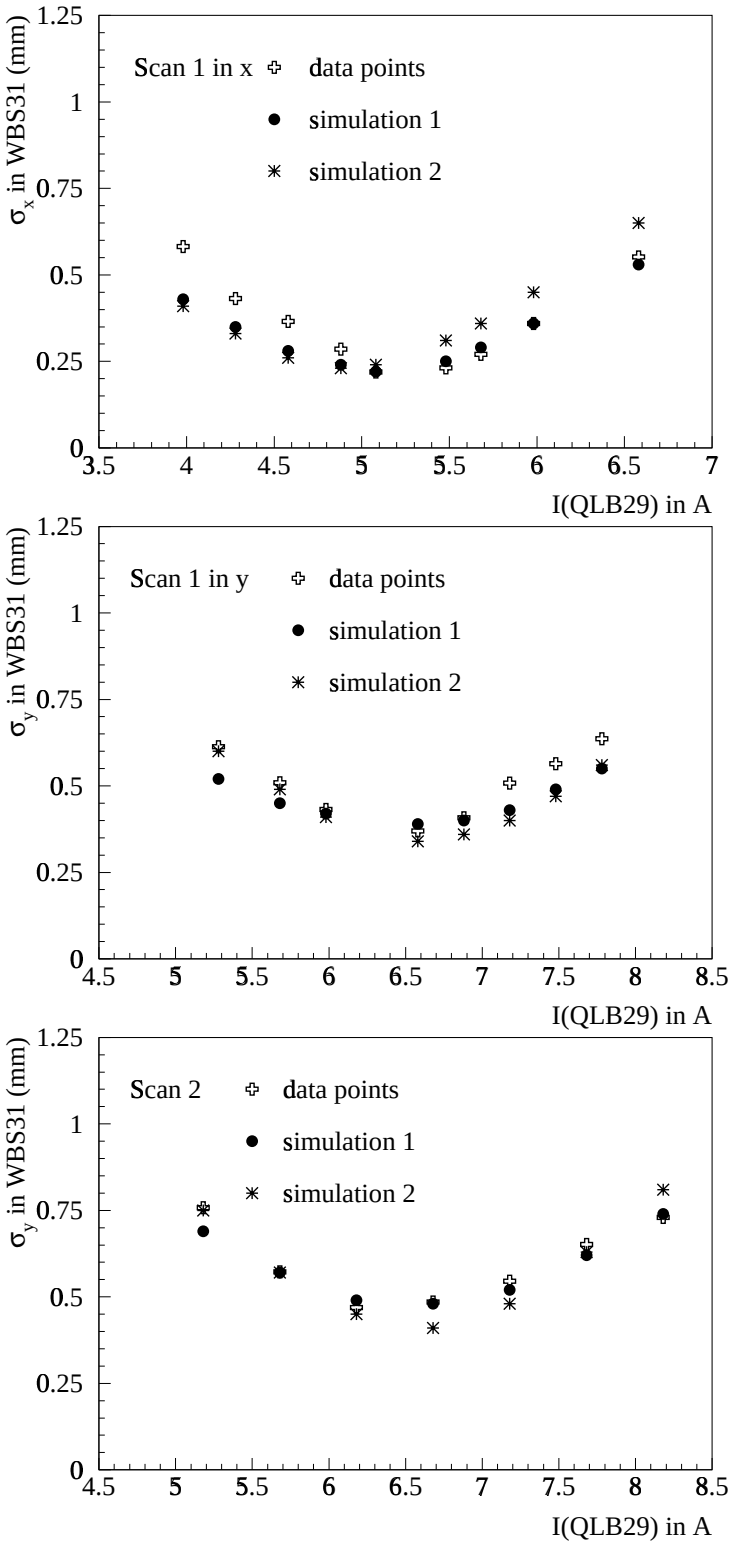

Figure 8: Transverse beam size in WL.WBS31 as a function of the current in WL.QLB29: the open crosses show the data points, while full circles and stars show the simulated points, when assuming an energy of 332 and 350 MeV in the matching section, respectively (simulation 1 corresponds to the 332 MeV case, and simulation 2 corresponds to the 350 MeV case).

7.4 Comparison with previous week quadrupole scans in WL.WBS31

During the previous week of operation, the same quadrupole scan in WL.WBS31 was performed in both planes using the quadrupole WL.QLB29. The beam conditions were similar to the ones used this week (peak power meter readings of 4.5, 33.2 and 34.9 MW on MDK25, MDK27 and MDK31 and same beam current). It is therefore interesting to compare the results in order to assess the reproducibility of the transverse conditions. Figure 9 shows the scans in the horizontal and vertical planes. They are compared to the results of this week. The points are the data measured last week, and the lines are the scans simulated by MAD using the initial Twiss parameters found this week in WL.QLB29 for an energy of 332 MeV at the end of the linac (See Table 3). In the vertical plane, the scans are very similar, whereas in the horizontal plane, we observe a discrepancy. Such measurements should be repeated to make sure that the optics we use in the matching section is well adapted to the optics in the linac.

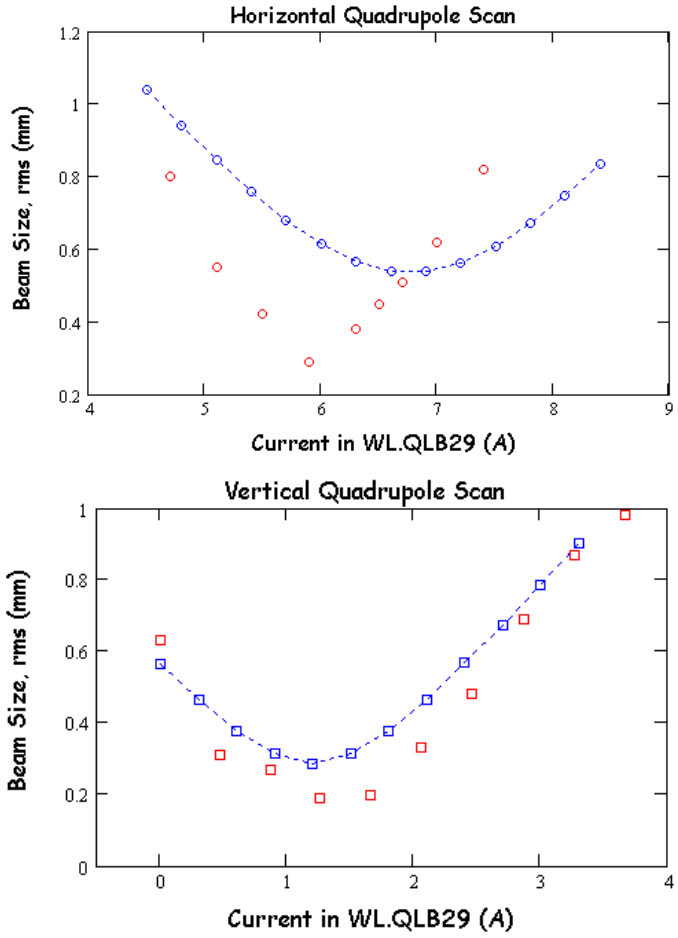

Figure 9: Horizontal and vertical quadrupole scans performed in WL.WBS31 during the previous week. The data are the points and the lines are the simulated scans using the Twiss parameters found this week.

7.5 The matching section

The measured Twiss parameters at the entrance of WL.QNF351 are different from the reference optics. In order to obtain the correct Twiss values at the reference location (point 0), one needs to adjust the five quadrupoles in the matching section. This was done for energies of 350 and 332 MeV with the respective initial conditions from Tab. 3. The results in Tab. 4 show that a matching can easily be obtained with currents that are not much different from the design values. In the case of 332 MeV, an alternative matching with lower currents is also given.

Quadrupole	design optics 350 MeV	rematched 350 MeV	rematched 332 MeV	alternative 332 MeV
WL.QNF351	70.0	87.7	86.8	68.2
WL.QNF352	72.6	87.5	85.6	37.0
WL.QNF353	54.3	54.3	51.5	0
WL.QNF371	162.8	159.8	151.7	145.2
WL.QNF372	198.0	199.3	188.8	186.8

Table 4: Quadrupole currents (in Ampere) in the matching section for the design optics and rematched with the initial conditions measured at the entry of WL.QNF351 for an energy of 350 MeV and 332 MeV. In addition, an alternative matching with lower currents at 332 MeV is shown.

During our studies, we noticed that the quadrupole WL.QNF351 seemed to be off-axis. Indeed, the beam was first aligned in the UMAs 34, 35, and 36, with all the quadrupoles and the correctors of the matching section on stand-by. When switching on WL.QNF351, we observed a displacement of -3 mm in UMA36. This is to be checked by survey people. In addition, we saw that the spectrometer magnet WL.BHZ36 has a non zero remanent field. Its effect prevents us from having a straight alignment of the beam in the matching section. Unfortunately, it is not possible to cycle the current in that bending magnet for the time being.

8 Trajectory Measurements

Trajectory measurements allow to compare the machine behaviour to the design optics. In the case of changing energy along a linear accelerator, the trajectory response $\Delta x(s)$ downstream a deflection by an angle $\Delta\theta$ at location s_0 depends on the Twiss functions and on the particle energy E as

$$\Delta x(s) = \sqrt{\beta(s)\ \beta(s_0)}\ \sin[\mu(s) - \mu(s_0)]\ \sqrt{\frac{E(s_0)}{E(s)}} \cdot \Delta\theta \tag{3}$$

where β and μ are the beta function and betatron phase, respectively. The beta function and the phase also depend on the energy since the normalised gradients for a given magnet current change inversely proportional to the particle momentum. So the trajectory response can be used to estimate the energy.

The measurement was done after having optimised the acceleration phases for peak power meter readings of 4.3, 33.1 and 34.5 MW on MDK25, MDK27 and MDK31, respectively. We used the correction coils WL.DQLA27V, WL.DQSA27.2H, WL.DQNF30.2H and WL.DQNF34.2H. For each of these correction trims a reference trajectory was measured by the UMA beam position monitors. The setting was changed while verifying that the transmission was not affected, and the difference to the reference was calculated. An example of a difference trajectory is shown in Figure 10.

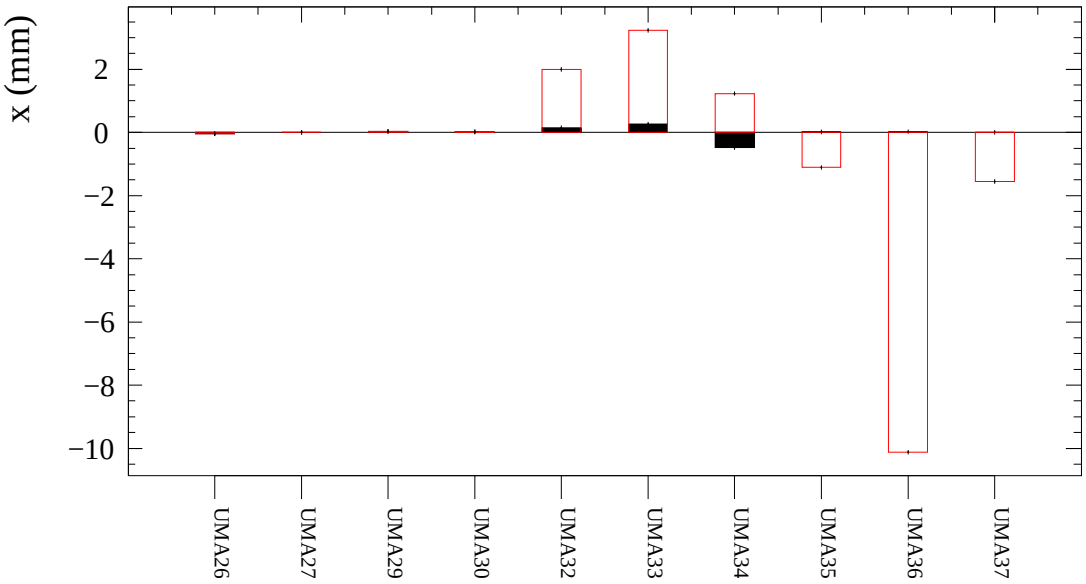

Figure 10: Horizontal difference trajectory (open bars) in the case of a 1 A current change on WL.DQNF30.2H. The expected trajectory change for an energy of 332 MeV at the linac exit is subtracted from this data. The residual difference (filled bars) has an RMS spread of 190 μm that is consistent with the noise of the UMAs.

The CTF3 machine was modelled with MAD taking into account the now known deviations from the design machine due to cabling errors and polarity inversions on the magnets. These made the horizontal beta function blow up between UMA36 and UMA37 so that the transmission was poor there. Therefore UMA37 was excluded from the analysis.

The measured data were compared to the theoretical trajectory response for different final energies at the end of the linac. The deflection angle of the trim was left as a free parameter since the calibration of the correction coils is probably not very precise. The residual RMS difference shows the discrepancy between model and data. Figure 11 shows this residual for the case of WL.DQNF30.2H. It is obvious that the model does not agree very well for an assumed energy of 350 MeV at the linac exit. The optimum correspondence indicates a final beam energy of about 331 MeV. This agrees very well with the beam energy measurement in the HIP and HIE lines (see Section 5.2). The influence of the energy at the trim location on the analysis was tested by varying the energy after accelerating section ACS30 (on which the trim is located) by ± 5 MeV. This sensitivity is smaller than for the final energy, as can be seen in Figure 11.

The trajectory change by WL.DQNF34.2H also corresponds to the model. The pattern is though not very sensitive to the energy in this case but the calculated deflection angle points to an energy of 331 MeV, as well.

Two measurements by WL.DQSA27.2H show a different phase advance for the two cases (probably related to the network zero crossing jumps, see section 3) and were not further analysed.

The analysis of WL.DQLA27V is very sensitive to the initial energy after the buncher. Unfortunately, UMA27 which is vital for this was not working during the measurement. Using the remaining UMAs, the comparison to the model was performed for different initial energies assuming a final energy of 332 MeV. This analysis shows the best agreement between model and data for an initial energy of about 2.8 MeV. Due to the UMA27 problem though, the result is not very conclusive and the measurement will have to be redone.

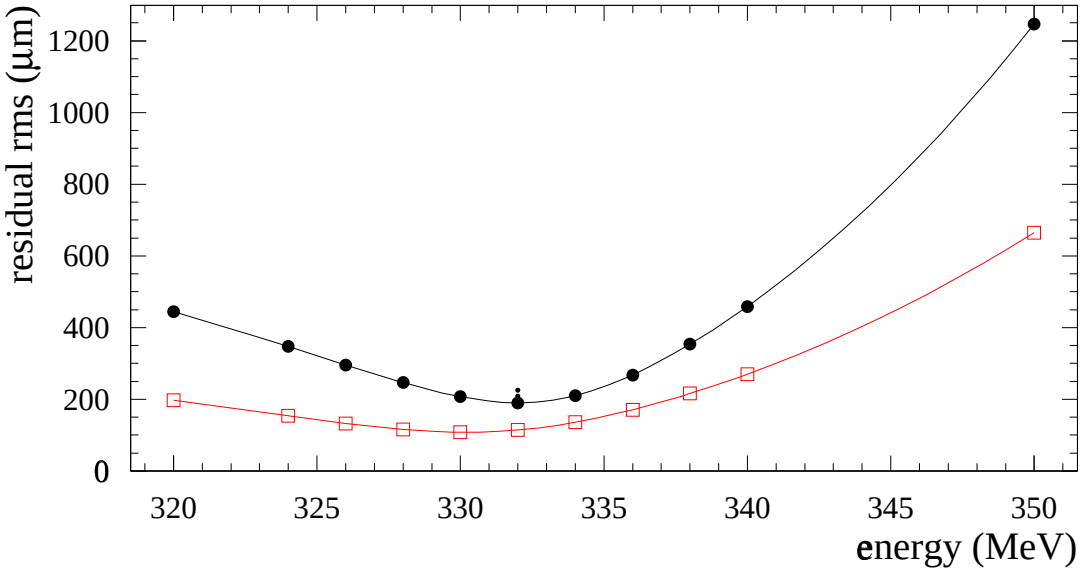

Figure 11: Residual trajectory difference between data and model as a function of the final beam energy at the exit of the linac. The two data sets correspond to two different current changes of WL.DQNF30.2H. The two small data points at the minimum of the black curve show the effect of a variation of the energy after ACS30 by ± 5 MeV. The best correspondence suggests a beam energy of 331 MeV.

9 Gun tests

During the week, we had problems starting the gun after an access, and the following days, the gun was frequently going to Off Pulsing. At the end of the week, new electronic cards were put in operation by the gun specialists. Two days were dedicated to perform the necessary tests. The current can now be varied between 50 mA and 1.8 A, with a variable pulse length between 2 ns and 10 ns, as required in the specifications. The details of the gun studies are available in the gun paper log-book.

10 Various Statements

During this week of operation, the following points have been noticed:

- The power supply WL.QNF371 dropped many times during the week. This was due to the control system which was sending a value to the single transceiver every basic period. This was fixed.
- The power supply HIE.QFW30 was dropping very often because of unstable electronic regulation. This was solved by PO.
- A preliminary measurement of the dispersion in the injection was carried out this week. Its analysis will be given in next week report, together with other dispersion measurements in HIE.

The research of A. Ferrari has been supported by a Marie Curie Fellowship of the European Community Programme ”Improving Human Research Potentiel and the Socio-economic Knowledge Base” under contract number HPMF-CT-2000-00865.

References

[1] R. Corsini, L. Rinolfi, T. Risselada, P. Royer, F. Tecker, “CTF3 Preliminary Phase Commissioning - Report on Second Week, 8-12 October 2001”, CTF3 Note 037, PS/AE Note 2001-016.

[2] R. Corsini, A. Ferrari, L. Rinolfi, T. Risselada, P. Royer, F. Tecker, “Beam Dynamics for the CTF3 Preliminary Phase”, CLIC Note 470.